Autonomous Spacecraft Formation Flying Implementation Near Mars Synchronous Orbit Based on Fuzzy Logic Control

BIYOGO NCHAMA Vicente Angel Obama^{1,2}, HASAN Mehedi³, MASUM Sajjad Hossain^{1,2}, SHI Peng^{1,2*}

- 1. School of Astronautics, Beihang University, Beijing 102206, P. R. China;
- 2. Key Laboratory of Spacecraft Design Optimization & Dynamic Simulation Technologies, Ministry of Education, Beijing 100191, P. R. China;
- 3. COMAC-Beihang Commercial Aircraft Innovation Center, Beihang University, Hangzhou 311115, P. R. China

(Received 18 June 2025; revised 20 August 2025; accepted 5 September 2025)

Abstract: In response to the need for a supportive on-orbit platform for future Mars exploration missions, this paper proposes the design and implementation of an autonomous spacecraft formation flying system near the Martian synchronous orbit using fuzzy learning-based intelligent control. A detailed analysis of spacecraft relative motion in the Mars environment is conducted, deducing the necessary conditions to reach the Martian synchronous orbit constraints. The modified Clohessy-Wiltshire (C-W) equation with Martian J_2 (Oblateness index) perturbation is used as a reference to design a fuzzy learning-based intelligent and robust nonlinear control approach, which helps to autonomously track the desired formation configuration and stabilizes it. An introduction to spacecraft propulsion mechanisms is provided to analyze the feasibility of using electrical thrusters for spacecraft formation configuration tracking and stabilization in Martian synchronous orbits. The simulations show the effectiveness of the proposed control system for long-term on-orbit operations and reveal its reliability for designing intelligent deep-space formation flying configurations, such as an autonomous Mars observatory, a Martian telescope, or an interferometer.

Key words: Mars space station; spacecraft formation flying; fuzzy logic-based spacecraft formation control; intelligent control

CLC number: V448 **Document code:** A **Article ID:** 1005-1120(2025)S-0001-11

0 Introduction

Mars is the fourth planet from the Sun and the nearest planet to the Earth that meets some of the fundamental living requirements^[1]. Implementing a spacecraft formation flying in Mars's synchronous orbit is the key for designing a supportive deep space structure for Mars exploration and interplanetary traveling^[2-3]. The main challenges for developing a formation flying near Mars's synchronous orbit are understanding the spacecraft dynamics in Martian orbits and implementing a reliable control strategy. Therefore, this paper uses the fuzzy-logic-based learning method to implement an autonomous

spacecraft formation flying system near Mars's synchronous orbit, which can serve as an intelligent Martian space or surface observatory or a deep space station for future Mars landing missions.

The successful landing of a manned spacecraft on Mars will represent a new chapter in space exploration^[1], as well as a big step in interplanetary traveling accomplishment^[4]. Since NASA's Marner4 visited Mars for the first time in 1965 and updated the human understanding of Mars' composition and environment^[1], several missions have aimed to explore and land on Mars. Notable examples include China's Tianwen mission, NASA's Curiosity Rov-

How to cite this article: BIYOGO NCHAMA Vicente Angel Obama, HASAN Mehedi, MASUM Sajjad Hossain, et al. Autonomous spacecraft formation flying implementation near mars synchronous orbit based on fuzzy logic control[J]. Transactions of Nanjing University of Aeronautics and Astronautics, 2025,42(S):1-11.

^{*}Corresponding author, E-mail address: shipeng@buaa.edu.cn.

er, and NASA's EscaPADE mission, among others.

In recent years, many researchers have presented feasible approaches to accomplish distinct Mars missions. To design and optimize the Earth-to-Mars transfer orbits, Liu et al.[3] analyzed the feasibility of transferring from Earth to Mars or from the Moon to Mars using Lambert's orbit transfer approach. They considered the relative motion of the planets to decide the best transfer time window for each case, providing a great reference for interplanetary traveling. For near-Mars orbit spacecraft designing and optimization, control, and engineering implementation, many researchers [4-11] used the classical control, optimal control, and reinforcement learning to provide a conceptual design of autonomous Mars spacecraft. For the successful landing and overall energy optimization of Mars' probes and rovers, researchers[12-14] presented a schematic algorithm to optimize the fuel consumption and analyzed the possibility of using a hybrid propulsion system for Mars exploration and landing. In summary, a successful Mars exploration depends on an accurate dynamical model and a robust control strategy. Although the design of Mars transfer orbits is extended in the literature, relatively few studies have been conducted to design a feasible Mars space station^[15].

To address this particular gap, this paper develops a fuzzy learning-aided intelligent, autonomous, and robust nonlinear control for spacecraft formation flying (SFF) implementation in the Mars synchronous orbit. The content of this paper is organized as follows. Section 1 provides a detailed analysis of SFF in Martian orbits. Section 2 introduces the basic concepts regarding electrical propulsion. Section 3 proposes a fuzzy learning-based robust nonlinear control for SFF control in Mars orbit, and its reliability is demonstrated through detailed fuzzy analysis. Section 4 uses two crafts to simulate the control system's performance.

1 Mathematical Modeling

Based on Mars' rigid surface, the motion of a spacecraft in a Mars orbit is an ideal two-body problem. Therefore, its assumptions are considered in

this preliminary analysis.

1.1 Relevant coordinate systems

- (1) Mars inertial frame $S_i(O_M x_i y_i z_i)$. The center O_M is at Mars' center of mass; the $O_M z_i$ axis is perpendicular to Mars' equatorial plane, pointing Mars-north. The $O_M x_i$ axis is located in Mars' equatorial plane, pointing to Mars' vernal equinox, and the $O_M y_i$ axis completes the right-hand coordinate system. The spacecraft's relative motion in this frame can refer to the geometry presented in Fig.1.
- (2) Co-linear frame $S_L(O_Ex_Ly_Lz_L)$. With the assumption of a two-body problem, this system can be considered as an inertial frame. Its center O_E is defined at Mars' center of mass. The O_Ex_L axis lies within the target craft's orbit plane (Fig.1), pointing to the Laplace constant vector. The O_Ez_L axis is perpendicular to the spacecraft orbit plane, and the O_Ey_L axis completes the right-hand system. The relative motion of spacecraft near Mars orbit can be represented in this frames as shown in Fig.1.

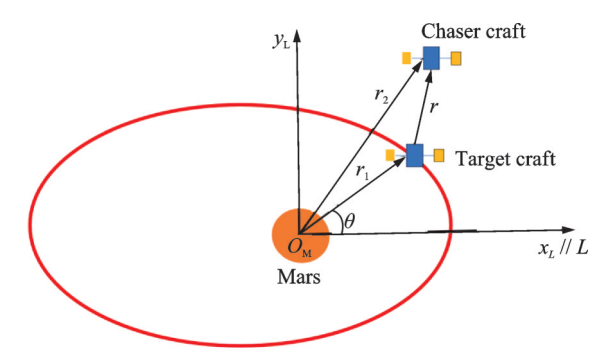


Fig.1 Spacecraft relative motion in near Mars orbit

(3) Target-craft system $S_{\rm T}(O_{\rm T}x_{\rm T}y_{\rm T}z_{\rm T})$ is the equivalent of the well-known local vertical local horizontal (LVLH) frame in Earth missions. The center $O_{\rm T}$ is defined at the target craft's center of mass, the $O_{\rm T}x_{\rm T}$ axis links Mars and the target craft. The $O_{\rm T}y_{\rm T}$ axis is parallel to target craft's tangential velocity. The $O_{\rm T}z_{\rm T}$ axis is perpendicular to the target craft's orbit plane. The rotational angle θ describes its relation with the co-linear frame.

1. 2 Relative motion modeling

Considering the solid composition of Mars and applying Newtonian mechanics $^{[15\text{-}18]}$, the dynamical motion of a spacecraft placed in near-Mars orbit can

be described in Mars' inertial frame $S_i(O_M x_i y_i z_i)$

$$\frac{d^{2}r_{j}}{dt^{2}} = -\mu_{M}\frac{r_{j}}{r_{j}^{3}} + a_{J_{2}j} + a_{Pj} + u_{j}$$
 (1)

where r_j is the jth spacecraft position vector concerning the center of Mars, $j=1,2,\cdots$, thus its norm is defined as $r_j = ||r_j||$; the vector a_{J_2j} is the J_2 perturbation term, i.e.

$$a_{J_{z}j} = -\frac{3J_{2}\mu_{\mathrm{M}}R_{\mathrm{M}}^{2}}{2r_{j}^{5}} \begin{bmatrix} \left(1 - 5\frac{z_{j}^{2}}{r_{j}^{2}}\right)x_{j} \\ \left(1 - 5\frac{z_{j}^{2}}{r_{j}^{2}}\right)y_{j} \\ \left(3 - 5\frac{z_{j}^{2}}{r_{j}^{2}}\right)z_{j} \end{bmatrix}$$
(2)

For Mars, the constant $J_2=1.960~45\times10^{-3}$. Furthermore, the vector $\boldsymbol{a}_{\rm Pj}$ represents other perturbations that affect Mars' spacecraft orbital motion. $\boldsymbol{u}_{\rm j}$ is the spacecraft orbit control acceleration. $\mu_{\rm M}=GM=4.283~4\times10^{13}~{\rm m}^3\cdot{\rm s}^{-2}$ is Mars' gravitational constant, i. e., $M=6.421~9\times10^{23}~{\rm kg}$ is Mars' mass, and $G=6.67\times10^{-11}~{\rm N}\cdot{\rm kg}^{-2}\cdot{\rm m}^2$ is the value of the universal gravitational constant. $R_{\rm M}$ is Mars' radius.

Based on Fig.1, the relative position vector of the chaser spacecraft concerning the target craft is $r = r_2 - r_1$, thus, the relative motion of the chaser with respect to the target is

$$\frac{\mathrm{d}^{2} \boldsymbol{r}}{\mathrm{d} t^{2}} = -\mu_{\mathrm{M}} \frac{\boldsymbol{r}_{1} + \boldsymbol{r}}{\|\boldsymbol{r}_{1} + \boldsymbol{r}\|^{3}} + \mu_{\mathrm{M}} \frac{\boldsymbol{r}_{1}}{\boldsymbol{r}_{1}^{3}} + \boldsymbol{a}_{J_{2}} + \boldsymbol{a}_{\mathrm{P12}} + \boldsymbol{u}_{12} (3)$$

Based on vectorial relative-derivation rules, the inertial acceleration or derivative term in Eq.(3) can be written in the LVLH system $S_{\rm T}(O_{\rm T}x_{\rm T}v_{\rm T}z_{\rm T})$ as^[18]

$$\frac{\mathrm{d}^{2} \boldsymbol{r}}{\mathrm{d} t^{2}} = \frac{\mathrm{d}_{\mathrm{T}}^{2} \boldsymbol{r}}{\mathrm{d} t^{2}} + 2\boldsymbol{\omega} \times \frac{\mathrm{d}_{\mathrm{T}} \boldsymbol{r}}{\mathrm{d} t} - \boldsymbol{r} \times \frac{\mathrm{d}_{\mathrm{T}} \boldsymbol{\omega}}{\mathrm{d} t} + \boldsymbol{\omega} \times (4)$$

$$(\boldsymbol{\omega} \times \boldsymbol{r})_{\mathrm{T}}$$

where ω is the rotational velocity of the LVLH coordinate system, i.e., the inertial frame. The subindex "T" states that the vector is expressed in the LVLH frame. Eq. (4) shows how to transform the derivative terms of the spacecraft dynamics from the inertial frame (left side) to the rotational system (right side). Therefore, Eq. (3) is described in the LVLH system as

$$\frac{\mathrm{d}_{\mathrm{T}}^{2} \boldsymbol{r}}{\mathrm{d}t^{2}} + 2\boldsymbol{\omega} \times \frac{\mathrm{d}_{\mathrm{T}} \boldsymbol{r}}{\mathrm{d}t} - \boldsymbol{r} \times \frac{\mathrm{d}_{\mathrm{T}} \boldsymbol{\omega}}{\mathrm{d}t} + \\ \boldsymbol{\omega} \times (\boldsymbol{\omega} \times \boldsymbol{r})_{\mathrm{T}} = -\mu_{\mathrm{M}} \left(\frac{1}{\|\boldsymbol{r}_{1} + \boldsymbol{r}\|^{3}} - \frac{1}{\|\boldsymbol{r}_{1}\|^{3}} \right) \boldsymbol{r}_{1} - \\ \mu_{\mathrm{M}} \frac{\boldsymbol{r}}{\|\boldsymbol{r}_{1} + \boldsymbol{r}\|^{3}} + \boldsymbol{a}_{J_{2}} + \boldsymbol{a}_{\mathrm{P12}} + \boldsymbol{u}_{12}$$
(5)

Hence, Eq.(5) provides a feasible reference for designing and analyzing the relative motion of two spacecraft when the target craft is moving in an elliptical orbit. Knowing that the operations between vectors should be referred to the same coordinate system, the sub-index "T" has been omitted in some terms of Eq.(5) for simplicity.

1.3 Modified C-W approach

Since the Mars-spacecraft system is considered as an ideal two-body problem. Thus, without loss of generality, in the preliminary analysis, it is reliable to co-nsider the colinear system $S_L(O_E x_L y_L z_L)$ as an inertial frame. Then, the orbital angular velocity is described in the LVLH frame as

$$\frac{\mathrm{d}}{\mathrm{d}t} \begin{bmatrix} 0 \\ 0 \\ \theta \end{bmatrix} = \boldsymbol{\omega} \tag{6}$$

SFF is a particular case of close-proximity relative motion, i.e., $\|r\| \ll \|r_1\|$. Thus, using the C-W approach, Eq.(5) is simplified into

$$\begin{cases} \ddot{x} - 2\omega \dot{y} - \omega^{2} x - \dot{\omega} y - 2\mu_{\rm M} x/r_{1}^{3} = + a_{J_{z}x} + u_{x} \\ \ddot{y} + 2\omega \dot{x} - \omega^{2} y + \dot{\omega} x + \mu_{\rm M} y/r_{1}^{3} = + a_{J_{z}y} + u_{y} \end{cases} (7)$$
$$\ddot{z} + \mu_{\rm M} z/r_{1}^{3} = + a_{J_{z}z} + u_{z}$$

where $\mathbf{u} = \begin{bmatrix} u_x & u_y & u_z \end{bmatrix}^T$ is the control on the chaser. Eq. (7) describes the motion of the chaser craft with respect to the target spacecraft in the LVLH coordinate system. Hence, assuming a cooperative relative motion, the orbital parameters of the target spacecraft can be calculated using the Kepler equation, i.e.

$$r_1 = \frac{p}{1 + e \cos \theta} \tag{8}$$

where $p = a(1 - e^2)$ is defined as the semi-latus rectum of the target craft orbit; a is the semi-major axis; e is the orbit eccentricity; and θ is the true anomaly angle, as shown in Fig.1.

1. 4 Mars synchronous orbit approach

A Mars synchronous orbit (MSO) is defined

as a circular orbit around Mars, in which the space-craft's orbital angular velocity is synchronized with Mars' rotational angular velocity. Based on Eq.(6), there is a constraint

$$\frac{\mathrm{d}_{\mathrm{R}}\boldsymbol{\omega}}{\mathrm{d}t} = 0 \tag{9}$$

Using Eq.(9), Eq.(7) becomes

$$\begin{cases} \ddot{x} - 2\omega \dot{y} - 3\omega^{2} x = a_{J_{z}x} + u_{x} \\ \ddot{y} + 2\omega \dot{x} = a_{J_{z}y} + u_{y} \\ \ddot{z} + \omega^{2} z = a_{J_{z}z} + u_{z} \end{cases}$$
(10)

Eq.(10) describes the motion of the chaser craft concerning the target craft, assuming that the target craft is moving in circular orbits. Thus, the angular velocity's norm satisfies

$$\omega^2 = \frac{\mu_{\rm M}}{r_1^3} = \frac{4\pi^2}{T^2} \tag{11}$$

For Mars' synchronous orbits, the target space-craft's orbital period should be T=24 h 40 min=88 642 s, thus

$$r_1 = \sqrt[3]{\frac{\mu_{\rm M} T^2}{4\pi^2}} = 20\,428\,{\rm km}$$
 (12)

Since $r_1 = r_M + h$, i.e., the "Mars to the target" radius is the sum of Mars' radius and the spacecraft altitude from Mars' surface. Therefore, the Mars synchronous orbit altitude is about h = 17053 km from Mars' surface.

2 Deep Space Propulsion

The propulsion system plays a key role in space mission design and implementation, enabling crucial maneuvers. The spacecraft's thrust is related to the propulsion system by

$$F = \dot{m}v_{\rm ex} = (\dot{m}_{\rm d} + \dot{m}_{\rm p})v_{\rm ex} = \dot{m}_{\rm p}v_{\rm ex} = \dot{m}_{\rm p}\frac{I_{\rm S}}{\sigma}$$
(13)

where $v_{\rm ex}$ is the propellant exhaust velocity; $\dot{m}_{\rm p}$ the propellant mass flow rate; $m_{\rm d}$ the dry mass, $I_{\rm S}$ the propulsion system's specific impulse; and g the equivalent gravitational acceleration at the considered near-Mars orbit altitude. In general cases, the specific impulse is a predefined parameter dependent on the properties of the propellant. The mass flow rate becomes the main control parameter to achieve the desired thrust.

For space exploration, electrical propulsion has

become a reliable option. Compared to the combustion-based chemical propulsion systems, the electrical propulsion systems use an electromagnetic field to accelerate particles and generate the required or command thrust. The thrust produced by an electrostatic propulsion system can be calculated as

$$F = \dot{m}_{\scriptscriptstyle D} v_{\scriptscriptstyle ex} \approx \dot{m}_{\scriptscriptstyle i} v_{\scriptscriptstyle i} = \dot{m}_{\scriptscriptstyle D} \eta_{\scriptscriptstyle m} v_{\scriptscriptstyle i} \tag{14}$$

where \dot{m}_i is the ions' flow rate; v_i is the ions' exhaust velocity; $\eta_m = \dot{m}_i/\dot{m}_p$ is defined as the propellant ionization efficiency or ionization rate. Furthermore, by conservation of energy applied to electrostatic and ionization, there is

$$qV_{\rm b} = \frac{1}{2} M v_i^2 \tag{15}$$

where $V_{\rm b}$ is the system's required voltage intensity to accelerate the ions. Therefore, the ionization rate becomes

$$\eta_{\scriptscriptstyle m} = \frac{\dot{m}_{\scriptscriptstyle i}}{\dot{m}_{\scriptscriptstyle D}} = \frac{I_{\scriptscriptstyle b}}{\dot{m}_{\scriptscriptstyle D}} \frac{M}{e} \tag{16}$$

where I_b is the system's required current intensity to accelerate the ions.

Therefore, the electrostatic thrust or force is

$$F = \gamma \sqrt{\frac{2M}{e}} I_{\rm b} \sqrt{V_{\rm b}} \tag{17}$$

Thus, the electrostatic thruster's specific impulse is

$$I_{\rm S} = \frac{F}{\dot{m}_{\rm p} g} = \frac{\gamma \eta_{\rm m} \sqrt{2 V_{\rm b} e / M}}{g} = \frac{1.65 \times 10^{-3} \gamma I_{\rm b} \sqrt{V_{\rm b}}}{\dot{m}_{\rm p} g}$$
(18)

The efficiency can be calculated as

$$\eta_{F} = \frac{P_{\text{jet}}}{P_{\text{in}}} = \frac{F^{2}}{2\dot{m}_{p}P_{\text{in}}} = \frac{P_{\text{jet}}}{I_{b}V} \cdot \frac{I_{b}V_{b}}{P_{\text{in}}} = \gamma^{2}\eta_{m}\eta_{e}$$
 (19)

where $P_{\rm jet}$ is the jet or propellant's power; $P_{\rm in}$ the system's input power; and $\eta_{\rm e}$ the electric system's efficiency. For Xe (Xenon) propellant, there is

$$F = 1.65 \times 10^{-3} \gamma I_{\rm b} \sqrt{V_{\rm b}} \tag{20}$$

Thus, its specific impulse is

$$I_{\rm S} = \frac{1.65 \times 10^{-3} \gamma I_{\rm b} / V_{\rm b}}{\dot{m}_{\rm p} g} \tag{21}$$

The main disadvantage of electrical propulsion is that the produced thrust is relatively smaller compared to the thrust produced by the chemical propellant.

3 Fuzzy Control Design

Fig. 2 shows the conceptual implementation of a fuzzy-logic-based intelligent control to implement an autonomous formation flying system. The main advantage of this method is that it provides intelligence and autonomy to the system to make intelligent decisions under random inputs^[19-21].

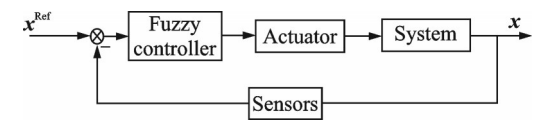


Fig.2 Conceptual implementation of intelligent formation flying

The challenge of the fuzzy-logic-based control strategy is that it is a learning-based control, in which the system control command is computed in three main steps: (1) Reference or input signals' fuzzification; (2) compute the best control action using the rules base; (3) control output's defuzzification to transform the fuzzy output into a deterministic signal that is sent to the actuator. The adopted fuzzy-logic-based control scheme is shown in Fig.3.

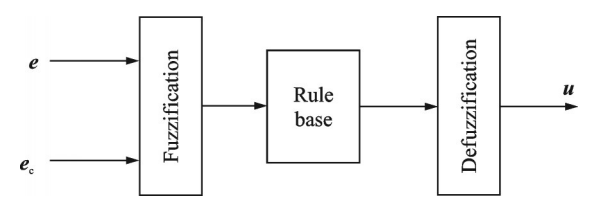


Fig.3 Fuzzy control strategy for two-craft state tracking

From the above description, it is evident that to use this controller for formation flying control in Mars synchronous orbit, it is required to train it previously using some reliable data or feasible "inputoutput" pairs. Thereby, this research assumes that some position error (e), velocity error (e), and the respective control outputs (u) are previously known.

3. 1 System analysis

Without loss of generality, the chaser space-craft's tracking state or reference state is defined as x^{Ref} , and the sensor's measured state is x, i.e.

$$x^{ ext{Ref}} = \begin{bmatrix} r^{ ext{Ref}} & v^{ ext{Ref}} \end{bmatrix}^{ ext{T}}$$
 , $x = \begin{bmatrix} r & v \end{bmatrix}^{ ext{T}}$

Therefore, the position error can be defined as $% \left(1\right) =\left(1\right) \left(1\right$

$$e = r^{\text{Ref}} - r \tag{22}$$

The velocity error or position error rate is de-

fined as

$$e_{c} = \dot{e} = \dot{r}^{Ref} - \dot{r} =$$

$$\dot{r}^{Ref} - \lim_{\Delta t \to 0} \frac{r(t + \Delta t) - r(t)}{\Delta t}$$
(23)

For a more representative approach, the velocity error has been written using the definition of differentiation. Based on the one-dimensional motion approach (Fig. 4)^[21], the possible configurations of a two-craft formation are analyzed, and then a more general control strategy is provided for the formation system control along the three axes.

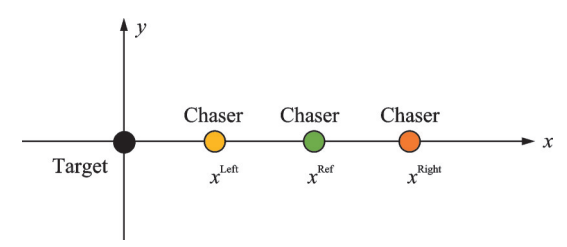


Fig.4 Formation flying one-dimensional state representa-

In Fig. 4, it is assumed that the target craft is placed at the origin of the coordinate system. Thus, considering a one-dimensional case along the $O_{\rm T}x_{\rm T}$ direction, the chaser can be in three possible positions, at the desired position $x^{\rm Ref}$, at the left of the desired position $x^{\rm Left}$, and at the right side of the desired position $x^{\rm Right}$. Thus, the control objective is to push the spacecraft to the desired position.

Therefore, for $e \in E$, $e_c \in E_c$, and $u \in U$, the signs of the control action are defined and analyzed, i.e., the positive control $u_x > 0$ to push the chaser craft from left to right (i.e., from the left side to the desired position), and the negative control action $u_x < 0$ to push the chaser craft from right to left (i.e., from the right side to the desired position). Based on that analysis, the state signals are defined, as shown in Table 1.

Based on state-error interpretation and the defined control signs, a preliminary control is proposed in Table 2.

Table 1 One-dimensional state error interpretation

Error	Interpretation
e > 0	The chaser is at the left, i.e., $x = x^{\text{Left}}$
e < 0	The chaser is at the right, i.e., $x = x^{\text{Right}}$
$e_{ m c}\!>\!0$	The chaser is moving to the left
$e_c < 0$	The chaser is moving to the right

Table 2 One-dimensional control rules

Condition	Action	
$e\!>\!0$ and $e_{\scriptscriptstyle m c}\!>\!0$	$u_x > 0$ and push to the right	
$e\!>\!0$ and $e_{\scriptscriptstyle m c}\!<\!0$	$u_x \geqslant 0$ and push to the right	
$e\!>\!0$ and $e_{\scriptscriptstyle \mathrm{c}}\!=\!0$	$u_x > 0$ and push to the right	
$e\!<\!0$ and $e_{\scriptscriptstyle \mathrm{c}}\!>\!0$	$u_x \leq 0$ and push to the left	
$e\!<\!0$ and $e_{\mathrm{c}}\!<\!0$	$u_x < 0$ and push to the left	
$e\!<\!0$ and $e_{\mathrm{c}}\!=\!0$	$u_x < 0$ and push to the left	
$e\!=\!0$ and $e_{\mathrm{c}}\!>\!0$	$u_x > 0$ and push to the right	
$e\!=\!0$ and $e_{\rm c}\!<\!0$	$u_x < 0$ and push to the left	
$e=0$ and $e_{\rm c}=0$	$u_x = 0$ and no action	

This analysis is feasible and general for the other three axes and any considered position vector, because if the chaser spacecraft position is a random vector \mathbf{r} , it is always feasible to compute its projection along each axis and then proceed with the same analysis.

3. 2 Fuzzification and control law

Although Table 2 provides a primary idea of how to implement the control action, it is still not accurate for training the two-craft formation flying to become intelligent and autonomous. Thus, for the state error e and the state error rate e_c along each axis, five-level linguistic values are defined, i.e., NB (Negative big), NS (Negative small), Z (Zero), PS (Positive small), and PB (Positive big). Thus, the following linguistic vectors are proposed

$$\begin{cases} e = [NB & NS & Z & PS & PB] \\ e_c = [NB & NS & Z & PS & PB] \end{cases}$$
 (24)

This research considers the membership functions, as shown in Fig.5, for the fuzzification of the relative motion state on each axis, i.e., position and velocity error.

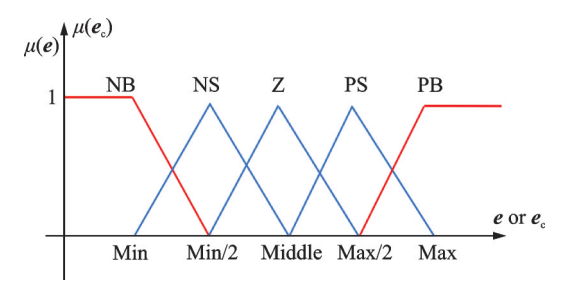


Fig. 5 Membership functions of e and e_0

Furthermore, for each axis control action μ , seven-level linguistic values are defined: NB (Negative big), NM (Negative middle), NS (Negative small), Z (Zero), PS (Positive small), PM (Positive small)

tive middle), and PB (Positive big). Thus, the linguistic vector is

$$u = [NB NM NS Z PS PM PB] (25)$$

This research considers the membership functions, as shown in Fig.6, for each axis control's fuzzification

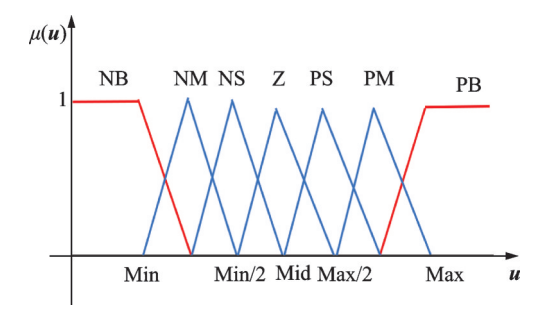


Fig.6 Membership functions of *u*

Therefore, based on the above analysis, a more accurate control strategy is defined, as shown in Table 3, to train the formation flying system to be intelligent and autonomous in terms of tracking the required relative motion state.

Table 3 Fuzzy control rules

			e		
<i>e</i> _c –	NB	NS	Z	PS	PB
NB	NB	NB	NB	PS	PB
NS	NB	NM	NM	PM	PB
Z	NM	NM	Z	PM	PB
PS	NM	NM	PM	PB	PB
PB	NS	NS	PB	PB	PB

Therefore, the accuracy of the control decision and the system's robustness depend on each of the defined trials or combination of e, e_c , u defined in Table 3.

3. 3 Fuzzy rules and defuzzification

For computing the required control action, this paper uses the Mamdani^[20] inference, which uses the known control system's input and output to train the controller to be able to autonomously generate a feasible and reliable control output for any random input using "if inputs, then outputs"^[20] rule base or inference. As mentioned previously, this research considers the fuzzy learning-based control scheme (Fig.3), and its control rule base is proposed in Table 3

Thereby, for the considered two-craft case, it is feasible to assume that some position and velocity

error inputs and the respective control outputs are known. Thus, suppose the trial e_k , e_{ck} and u_k belongs to the feasible state and control space, then $e_k \wedge e_{ck} \rightarrow u_k$ corresponds to the related Mamdani inference^[20], i.e., the rule is

$$\boldsymbol{R}_{k} = (\boldsymbol{e}_{k} \times \boldsymbol{e}_{ck})^{\mathrm{T}_{1}} \times \boldsymbol{u}_{k} \quad k = 1, 2, \cdots$$
 (26)

where T_1 is a vectorization operator that denotes the vectorization^[20] of the computed cartesian product $e_k \times e_{ck}$ by concatenating its rows to form a column vector. Thereby, the resultant inference is defined as the composition product of all independent inferences, i.e.,

$$R = R_1 \circ R_2 \circ R_3 \circ R_4 \circ \cdots \circ R_k \circ \cdots \tag{27}$$

where " \circ " stands for the fuzzy compound calculation^[20]. Thus, for any newly defined inputs e_{new} and e_{cnew} , the corresponding control output is

$$\boldsymbol{u}_{\text{new}} = (\boldsymbol{e}_{\text{new}} \times \boldsymbol{e}_{\text{cnew}})^{\text{T}_2} \times \boldsymbol{R}$$
 (28)

where T_2 is a vectorization^[20] operator that denotes the vectorization of the Cartesian product $e_{\text{new}} \times e_{\text{cnew}}$ by concatenating its columns to form a row vector.

Furthermore, the Mamdani inference can be computed by the known input and output membership functions. Thus, instead of computing Eq.(28), it is reliable to just compute the equivalent membership written form^[20], i.e.

$$\mu_{\mu_{\text{new}}}(U) = \bigvee_{E,E_c} \left[\mu_{((e_{\text{new}} \times e_{\text{cnew}})^{T_z})}(E,E_c) \wedge \mu_R(E,E_c,U) \right]$$
(29)

The control output computed by Eqs. (28, 29) is a fuzzy vector, and its defuzzification into a deterministic signal that can be input to the actuator is required. In this research, the value corresponding to the centroid^[20] of the fuzzy output vector is considered as the deterministic control action.

4 Simulation and Analysis

Fig.7 shows the simulation step of the control procedure for a hypothetical mission implementation.

The following state-space variables are defined

$$x_1 = x, x_2 = y, x_3 = z$$

 $x_4 = \frac{dx}{dt}, x_5 = \frac{dy}{dt}, x_6 = \frac{dz}{dt}$

Thus, Eq.(10) can be rewritten in state-space

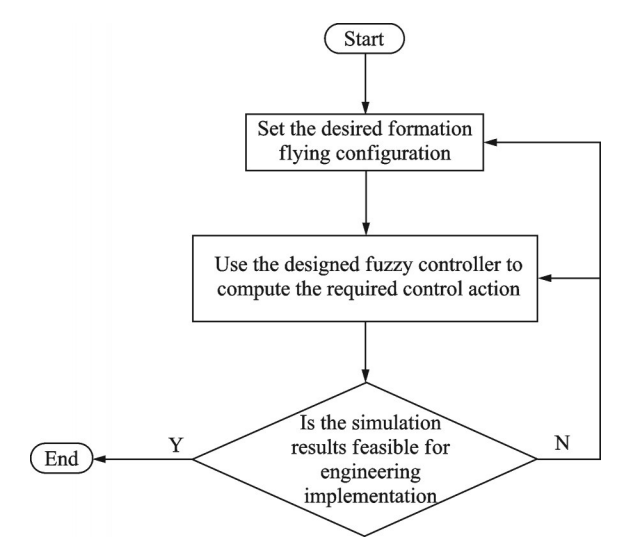


Fig.7 System's simulation step

form as

$$\begin{cases} \frac{\mathrm{d}x}{\mathrm{d}t} = Ax + Ba_{J_z}(x) + v + Bu \\ y = Cx + w \end{cases}$$
 (30)

In the preliminary analysis, it is assumed that the dynamics and the output noise can be neglected, i.e., v = 0, w = 0, and

$$x = \begin{bmatrix} x_1 \\ x_2 \\ x_3 \\ x_4 \\ x_5 \\ x_6 \end{bmatrix}, C = I_{6 \times 6}; B = \begin{bmatrix} 0 & 0 & 0 \\ 0 & 0 & 0 \\ 0 & 0 & 0 \\ 1 & 0 & 0 \\ 0 & 1 & 0 \\ 0 & 0 & 1 \end{bmatrix}, u = \begin{bmatrix} u_1 \\ u_2 \\ u_3 \end{bmatrix}$$

Consequently, the system matrix becomes

$$A = \begin{bmatrix} 0 & 0 & 0 & 1 & 0 & 0 \\ 0 & 0 & 0 & 0 & 1 & 0 \\ 0 & 0 & 0 & 0 & 0 & 1 \\ 3\omega^2 & 0 & 0 & 0 & 2\omega & 0 \\ 0 & 0 & 0 & -2\omega & 0 & 0 \\ 0 & 0 & -\omega^2 & 0 & 0 & 0 \end{bmatrix}$$

Furthermore, the parameters of the considered spacecraft for this simulation and analysis are shown in Table 4.

Table 4 Mars orbit spacecraft parameters

Parameter	Value	
Spacecraft mass/kg	50	
Propulsion system	Electrical	
Orbit type	Mars synchronous (MSO)	
Orbit inclination/(°)	0	
Target craft's orbit altitude/km	20 428	
Orbit period/s	88 642	

The desired or tracking state vector is

$$\boldsymbol{x}^{\text{Ref}} = \begin{bmatrix} \boldsymbol{r}^{\text{Ref}} \\ \boldsymbol{v}^{\text{Ref}} \end{bmatrix} = \begin{bmatrix} 0 \\ -100 \\ 0 \\ 0 \\ 0 \\ 0 \end{bmatrix}$$
(31)

This means the main goal is to force the chaser craft to track a relative distance of 100 m behind the target craft. This has important implications in engineering, being key for the terminal rendezvous motions. One can simulate the system for any initial state. This research assumes proximity relative motion constraints and, therefore, defines the initial state

$$\boldsymbol{x}^{\text{Initial}} = \begin{bmatrix} \boldsymbol{r}^{\text{Initial}} \\ \boldsymbol{v}^{\text{Initial}} \end{bmatrix} = \begin{bmatrix} 10 \\ -200 \\ 10 \\ 0 \\ 10 \\ 1 \end{bmatrix}$$
(32)

Thereby, the next simulations show the performance of the system in tracking tangential formation configuration constraints given in Eq.(31), when the chaser craft is departing from the arbitrary state defined in Eq.(32). Table 5 provides the length of the considered domain for each of the membership functions in the three axes.

Table 5 Membership function domain

Vector	Min	Middle	Big
e	-800 m	0	+800 m
$\boldsymbol{e}_{\mathrm{c}}$	$-80~\mathrm{m/s}$	0	+80 m/s
u	-8 m/s^2	0	$+8 \text{ m/s}^2$

Based on the above constraints, the following results first simulate the designed fuzzy learning-based controller's performances (Fig.8). As shown in the control surface, the minimal zero control action corresponds to the reference or steady state, and the extremal control corresponds to the cases in which the chaser craft tends to deviate too much from the tracking state. The direct interpretation of these results is that the defined control rules and the corresponding linguistic variables match the basic requirements of a reliable autonomous control system. In other words, the control rule base given in Table

3 is reliable for implementing autonomous relative motions. Thus, this approach is feasible for longterm formation flying control. Providing a reference rule base for the design and engineering implementation of fuzzy learning-based cooperative relative motion.

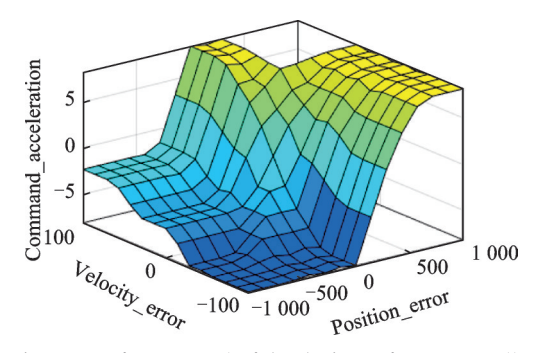


Fig.8 Surface control of the designer fuzzy controller

The performances of the formation flying system along each axis are shown in Figs. 9—17. The simulation results show that the designed fuzzy controller performs effectively, driving the chaser spacecraft to the desired state and simultaneously stabilizing the formation flying system autonomously. The time response shows that the system requires nearly 1 min to achieve the required state, which is considered as a smooth performance given the case that the chaser has been driven from an arbitrary initial state and the control action is also bounded within 1 m/s^2 .

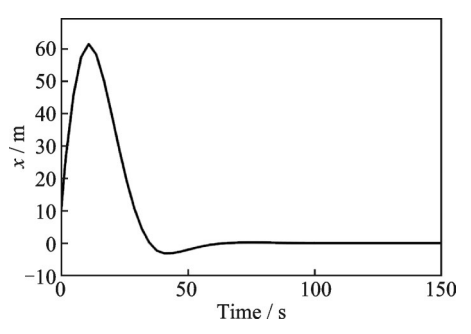


Fig. 9 Relative position response along x direction

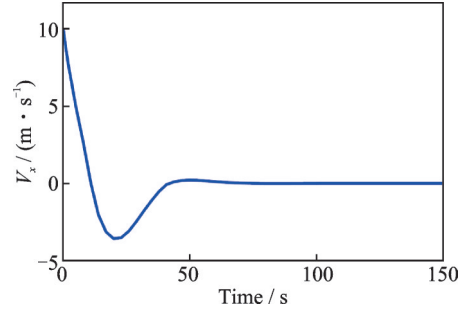


Fig. 10 Relative velocity response along x direction

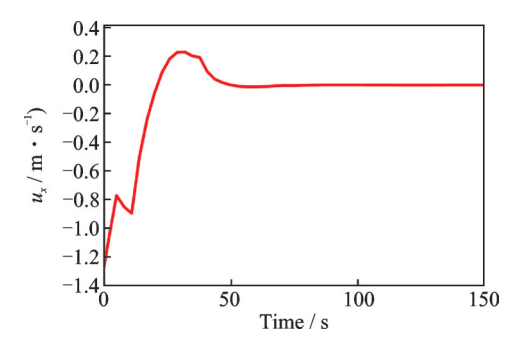


Fig.11 Command control acceleration along x direction

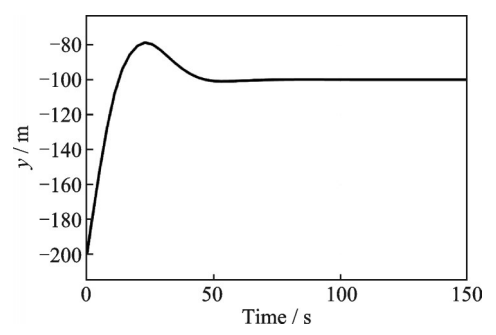


Fig.12 Relative position response along y direction

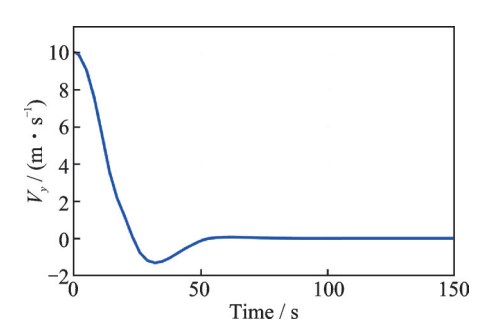


Fig.13 Relative velocity response along y direction

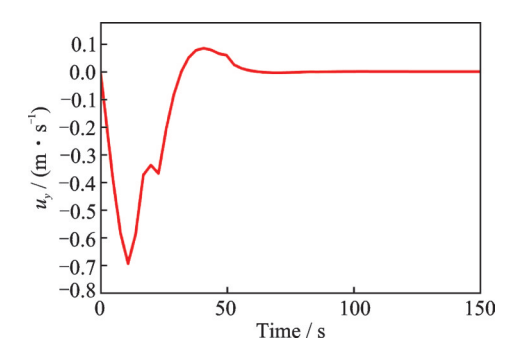


Fig.14 Command control acceleration along y direction

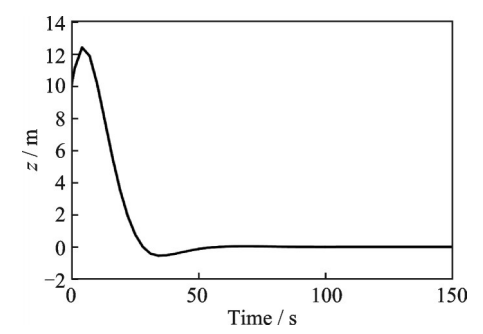


Fig.15 Relative position response along z direction

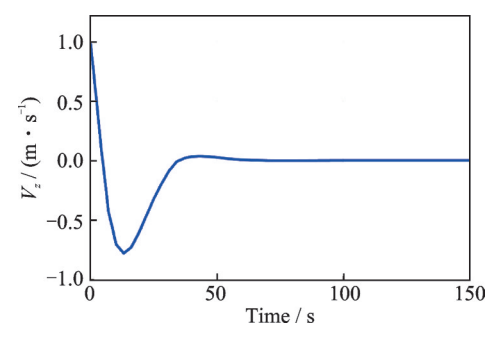


Fig.16 Relative velocity response along z direction

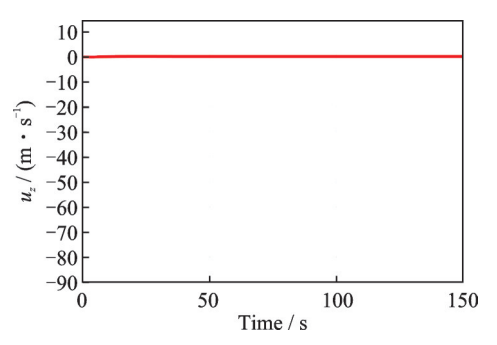


Fig.17 Command control acceleration along z direction

Further observations on the control response on each axis reveal that it is within the range that can be achieved by low-thrust, such as the electrical propulsion systems introduced in Section 2. Additionally, the simulations reveal that the control in the x direction is more aggressive than in other axis directions, which is understandable regarding the defined initial state. Thus, these results demonstrate the reliability and effectiveness of the proposed control mechanism for an autonomous Mars space station design, proving its potential for engineering applications.

Furthermore, since the same control strategy is used to control the relative motion on each axis, the time response and the convergence of the simulation results confirm the reliability of the conducted analysis and the great learning performance of the designed fuzzy logic-aided intelligent control system. From a data-driven control perspective, these simulations assert the feasibility of using fuzzy-logic-based intelligent control to implement an autonomous formation flying system in Mars synchronous orbit. Therefore, this can be considered an effective nonlinear control approach for SFF control.

Since the proposed fuzzy aided control rule base does not depend on the system dynamics, and the J_2 perturbation has been considered in the simula-

tions, it is concluded that this control strategy is robust under uncertainties and satisfies the autonomous control requirements.

5 Conclusions

This paper conducts a comprehensive analysis on the design and engineering implementation of an autonomous SFF system in Mars synchronous orbit, using a fuzzy learning-aided intelligent control system and low-thrust technology. This is a key idea for Mars space station design and deep space exploration. The simulation results reveal the feasibility, reliability, and effectiveness of the proposed control mechanism for long-term operations on Martian orbits. providing a valuable reference for the use of data-driven controllers in deep space exploration. This research is conducted in three main steps.

- (1) A detailed analysis of the spacecraft's motion in near-Mars orbit is conducted. The Martian synchronous orbit approach is derived, and the modified C-W equation with Martian J_2 perturbation is used to describe the spacecraft formation flying in Martian orbits.
- (2) The basic idea behind fuzzy control is described, and then the fuzzy logic method is used to design an intelligent controller, and the formation flying is trained to be autonomously controllable under uncertainty.
- (3) The basic space propulsion principles are introduced to analyze the feasibility of the idea for real mission design and implementation. The simulation results agree with the proposed theoretical design. Therefore, this research satisfies the primary engineering needs of autonomous systems.

This research shows the potential of using a data-driven control method to implement formation flying in Mars synchronous orbit. Thus, our next objective is to delve into the design of a multi-spacecraft autonomous formation in Mars orbit using data-driven control.

References

- [1] ZHAO Y S, ZHOU D S, LI X Y, et al. The evolution of scientific goals for Mars exploration and future prospects[J]. Chinese Science Bulletin, 2020, 65 (23): 2439-2453.
- [2] ISENI P, HALILI F. Reliable service-oriented archi-

- tecture for NASA's Mars exploration rover mission[C]//Proceedings of 2022 11th Mediterranean Conference on Embedded Computing (MECO). Montenegro, Canada; IEEE, 2022; 1-5.
- [3] LIU C M, JUANG J C. Orbit transfer from earth to Mars using modified Lambert algorithm[C]//Proceedings of 2016 International Automatic Control Conference (CACS). Taipei, China: IEEE, 2016: 155-160.
- [4] SOPEGNO L, VALAVANIS K P, RUTHER-FORD M J, et al. Mars sample return mission: Mars ascent vehicle propulsion design[C]//Proceedings of 2020 IEEE Aerospace Conference. Big Sky, USA: IEEE, 2020: 1-9.
- [5] MENGGEN S, CUI P Y, ZHU S Y. Networked Mars satellite system design and autonomous navigation analysis[C]//Proceedings of the 26th Chinese Control and Decision Conference. Changsha, China: IEEE, 2014: 3316-3321.
- [6] CHAI R Q, SAVVARIS A, TSOURDOS A, et al. A review of optimization techniques in spacecraft flight trajectory design[J]. Progress in Aerospace Sciences, 2019, 109: 100543.
- [7] GAO J S, LIU L, WANG Y J. Spacecraft orbit design based on intelligent optimization[C]//Proceedings of 2017 2nd International Conference on Advanced Robotics and Mechatronics. Hefei, China: IEEE, 2017; 681-687.
- [8] YOUNSE P J, CAMERON J E, BRADLEY T H. Comparative analysis of model-based and traditional systems engineering approaches for architecting a robotic space system through automatic information transfer[J]. IEEE Access, 2021: 107476-107492.
- [9] KARP A. Hybrid rocket propulsion for a low temperature mars ascent vehicle[D]. Pasadena, USA: California Institute of Technology.
- [10] VADIM Z, VLADIMIR P. Russian nuclear rocket engine design for Mars exploration[J]. Tsinghua Science and Technology, 2007, 12(3): 256-260.
- [11] YANG J, LIS, LIC, et al. Multi-objective optimization of landing fuel strategy for Mars exploration rover[J]. Aerospace Science and Technology, 2021, 118: 106258.
- [12] LIU W, FENG Y, LUO Y. Landing fuel consumption optimization of Mars rover based on improved genetic algorithm [J]. Journal of Harbin Institute of Technology, 2021, 53(3): 129-134.
- [13] HUANG Q, CHEN L, XIE Y. A fuel optimization approach for Mars rover descent and landing based on Monte Carlo Tree Search[J]. Aerospace Science and Technology, 2021, 116: 106110.
- [14] LIN RG, XUQC, WANGZA, et al. Optimization

scheme for landing fuel of Mars probe[C]//Proceedings of 2023 5th International Conference on Industrial Artificial Intelligence. Shenyang, China: IEEE, 2023: 1-5.

- [15] KUO N R. Mars network operations concept[C]// Proceedings of 2000 IEEE Aerospace Conference. Big Sky, USA: IEEE, 2000: 209-216.
- [16] NCHAMA V A O B, SHI P, MASUM S H, et al. Spacecraft dynamics linearizing and optimal control based on operational research and LQI[C]//Proceedings of 2024 21st International Bhurban Conference on Applied Sciences and Technology. Murree, Pakistan: IEEE, 2024; 294-299.
- [17] QUADRELLI M B. Spacecraft dynamics and control: An introduction[J]. IEEE Control Systems Magazine, 2015, 35(2): 103-106.
- [18] ZHAO Yushan, SHI Peng. Modeling theory and method of spacecraft flight dynamics[M]. Beijing: Beihang University Press, 2012. (in Chinese)
- [19] JUANG J G, LIN R W, LIU W K. Comparison of classical control and intelligent control for a MIMO system[J]. Applied Mathematics and Computation, 2008, 205(2): 778-791.
- [20] LIU Jinkun. Intelligent control theoretical basis, algorithmic design and application[M]. Beijing: Tsinghua University Press, 2022. (in Chinese)
- [21] VICENTE ANGEL OBAMA B N, AKRAM H M, YE Y K, et al. Intelligent path programming approach for autonomous ecological vehicles based on fuzzy log-

ic control[J]. Journal of Physics: Conference Series, 2025, 3041(1): 012031.

Acknowledgements This work was supported by the National Laboratory of Space Intelligent Control (No.HT-KJ2023KL502007); and the Chinese Government Scholarship (CSC).

Authors

The first author Mr. BIYOGO NCHAMA Vicente Angel Obama is currently a Ph.D. candidate in School of Astronautics, Beihang University. His research focuses on intelligent control of spacecraft, spacecraft dynamics, and spacecraft formation flying.

The corresponding author Prof. SHI Peng is a full professor at School of Astronautics, Beihang University. His research focuses on spacecraft dynamics, spacecraft design, and spacecraft control.

Author contributions Mr. BIYOGO NCHAMA Vicente Angel Obama conceptualized the idea, wrote the first draft of the manuscript, and conducted numerical verifications. Dr. HASAN Mehedi conducted research validation and methodology verification. Mr. MASUM Sajjad Hossain assisted with the literature review and paper revisions. Prof. SHI Peng conducted overall supervision and final verification. All authors commented on the manuscript draft and approved the submission.

Competing interests The authors declare no competing interests.

(Production Editor: ZHANG Bei)

基于模糊逻辑控制的火星同步轨道附近自主航天器编队 飞行研究

BIYOGO NCHAMA Vicente Angel Obama^{1,2}, HASAN Mehedi³, MASUM Sajjad Hossain^{1,2},炉 鹏 ^{1,2}

(1.北京航空航天大学宇航学院,北京100191,中国;2.航天器设计优化与动态模拟技术教育部重点实验室,北京100191,中国;3.大飞机科创中心/大飞机研究院,杭州311115,中国)

摘要:针对火星探测任务的在轨支持平台需求,提出了一种基于模糊逻辑学习的火星同步轨道附近的自主航天器编队飞行智能自适应控制方法。对火星环境中的航天器相对运动进行了详细分析,并推导出实现火星同步轨道约束的必要条件。随后,采用考虑火星扁率指数 (J_2) 摄动的修正Clohessy-Wiltshire(C-W)方程作为参考模型,设计了一种基于模糊学习的智能以及高鲁棒非线性控制器,该控制器能够自主跟踪期望的编队构型并使其稳定。随后介绍了航天器推进机理,有助于分析在火星同步轨道上使用电推进器进行航天器编队构型跟踪与保持的可行性。仿真结果展示了所提出控制系统在长期任务中的有效性,并验证了其在设计诸如自主火星观测站、火星望远镜或干涉仪等智能深空编队飞行构型方面的可靠性。

关键词:火星空间站;航天器编队飞行;基于模糊逻辑的航天器编队控制;智能控制